# Modeling ionospheric outflows and their impact on the magnetosphere, initial results

A. Glocer,[1] G. Tóth,[2] T. Gombosi,[2] and D. Welling[2]

Received 6 January 2009; revised 19 March 2009; accepted 31 March 2009; published 27 May 2009.

[1] Ionospheric outflow has been shown to be a significant contributor to the plasma population of the magnetosphere during active geomagnetic conditions. We present the results of new efforts to model the source and effects of out-flowing plasma in the Space Weather Modeling Framework (SWMF). In particular, we develop and use the Polar Wind Outflow Model (PWOM), a field-aligned, multifluid, multifield line polar wind code to simulate the ionospheric outflow. The PWOM is coupled to the ionosphere electrodynamics and global magnetosphere components of the SWMF, so we can calculate the outflow and its resulting impact on magnetospheric composition and dynamics. By including the outflow as part of a coupled system, we study the consequences of outflow on the larger space environment system. We present our methodology for the magnetosphere-ionosphere coupling, as well as the effect of outflow on the magnetosphere during two geomagnetic storms. Moreover, we explore the use of multispecies MHD to track the resulting plasma composition in the magnetosphere. We find that, by including ionospheric outflow during geomagnetic storms, we can reduce the RMS error in the simulated magnetic field as compared with various GOES satellites by as much as 50%. Additionally, we find that the outflow causes a strong decrease in Dst and in the cross-polar cap potential.

**Citation:** Glocer, A., G. Tóth, T. Gombosi, and D. Welling (2009), Modeling ionospheric outflows and their impact on the magnetosphere, initial results, *J. Geophys. Res.*, *114*, A05216, doi:10.1029/2009JA014053.

## 1. Introduction

[2] Magnetosphere-ionosphere coupling (MIC) is an intricate process involving electrical connectivity and mass flow. Energetic electrons and protons precipitate into the ionosphere from the magnetosphere creating local ionization, heating, aurora and airglow. Mass can also flow from the ionosphere to the magnetosphere. The complicated nature of MIC makes it very difficult to include in numerical models.

[3] Most global magnetosphere models have an inner boundary between 2 and 3 Earth radii. The upper boundary of most ionospheric models only extend up to 1000 km at most. Between these two regions, there exists a modeling gap that is often ignored. The gap includes plasmaspheric, auroral, and polar cap field lines, and it is through this region that plasma is accelerated into the magnetosphere providing a source of ionospheric plasma.

[4] There are a preponderance of data studies that demonstrate the relative contribution of ionospheric plasma, entering the magnetosphere through the gap, to make up a significant fraction of the magnetospheric plasma population. Indeed, the first measurements of $O^+$ ions in the magnetosphere by *Shelley et al.* [1972] illustrated the role that the ionosphere can play as a source to the magnetosphere. *Nosé et al.* [2003] used data from the Energetic Particle and Ion Composition (EPIC) instrument on-board the Geotail spacecraft to examine the $O^+/H^+$ energy density ratio in the plasma sheet during geomagnetic storms. They found that the ratio can reach 0.3–1.0 at the peak of a storm. Moreover, *Nosé et al.* [2005] found that during the extreme case of the 29–30 October 2003 superstorm, the $O^+/H^+$ energy density ratio reached 10–20 at the storm maximum. A review paper by *Daglis et al.* [1999] compiled relative magnetosphere ring current composition based on the Active Magnetospheric Particle Tracer Explorer (AMPTE) mission of the 1980s and the Combined Release and Radiation Effects Satellite (CRRES) observations; they summarized ring current composition measurements during varying conditions and showed increased oxygen ions present during active periods. *Pulkkinen et al.* [2001] used data from the Polar spacecraft and demonstrated that the $O^+$ energy density increases with solar variability whereas $H^+$ and $He^+$ energy densities do not. Another study by *Sharp et al.* [1985] examined International Sun-Earth Explorer (ISEE) 1 satellite and Spacecraft Charging AT High Altitude (SCATHA) satellite mass spectrometer data and found the ionosphere to be an important or dominant source of plasma for the inner magnetosphere. Additionally, *Huddleston et al.* [2005] examined data from Dynamics Explorer and Polar satellites, and also found the ionosphere to be a sufficient source for magnetospheric plasma. *Moore* [1984] review the

[1]NASA/GSFC, Greenbelt, Maryland, USA.
[2]Department of Atmospheric Oceanic and Space Sciences, University of Michigan, Ann Arbor, Michigan, USA.


0148-0227/09/2009JA014053

evidence of ion acceleration and heating at low altitudes and the impact on outflow. These data studies, and others not included here, illustrate the importance of including the ionospheric impacts on the space environment system. For a complete tutorial of the role of $O^+$ in MIC, please refer to the work of *Lotko* [2007].

[5] Of course, the ionosphere is also affected by external sources. A paper by *Abe et al.* [2004] examined the Akebono suprathermal ion mass spectrometer observations to quantify the impact of varying solar input on polar wind type ionospheric outflow. They indeed found that there was significant dependence on solar input (characterized by the 10.7 cm solar radio flux known as the F10.7 index). This result compares well with earlier numerical studies [*Cannata and Gombosi*, 1989; *Gombosi et al.*, 1991]. The topside electron heat flux, which represents direct magnetosphere energy input, also affects the outflow solution. *Bekerat et al.* [2007] carried out a study to find the range of values that allow their model to best match data taken by the Defense Meteorological Satellites Program (DMSP) satellite. Those values for topside heat flux fall into the range of $0.5–1.5 \times 10^{10}$ eV cm$^{-2}$ s$^{-1}$.

[6] With such a preponderance of evidence supporting the importance of MIC, it is imperative to look at how these processes are currently included in large scale models. The electrical connectivity between the ionosphere and magnetosphere is usually treated in a similar manner in different models [*Wang et al.*, 2008; *Wiltberger et al.*, 2004; *Ridley et al.*, 2004]. Typically, a height integrated conductivity is calculated by the ionosphere model which is combined with the Field Aligned Current (FAC) information from the magnetosphere model. The resulting calculation gives the polar cap potential.

[7] Unlike the electrical connectivity in MIC, mass coupling is handled very differently in different models. *Zhang et al.* [2007] changed the inner boundary density of the BATS-R-US (Block-Adaptive-Tree Solar wind Roe-type Upwind Scheme [*Powell et al.*, 1999; *De Zeeuw et al.*, 2000; *Gombosi et al.*, 2001]) magnetosphere model to represent changing amounts of mass flowing from the ionosphere to the magnetosphere. In this case the plasma is drawn off the inner boundary by pressure gradients. They found that the calculated Dst index is sensitive to the value chosen. Another approach is taken by *Gagne* [2005] who used an empirical relationship relating oxygen outflow developed by *Strangeway et al.* [2000] to set the inner boundary density of the Lyon-Fedder-Mobarry (LFM [*Lyon et al.*, 2004]) magnetosphere model in the following manner. The study by *Strangeway et al.* [2000] relates the Poynting flux with cusp related oxygen ion outflow. *Gagne* [2005] calculated the Poynting flux in the LFM code, mapped the results to Fast Auroral SnapshoT explorer (FAST) satellite altitudes, assumed the cusp relationship holds over the entire polar cap, and then set the boundary accordingly. A similar approach was also used by *Moore et al.* [2007]. *Winglee* [2000] used yet another approach. He used centrifugal acceleration of ions to throw plasma off the inner boundary. Then their multifluid MHD model tracked the out-flowing ionospheric plasma in order to define a geopause where the magnetosphere is dominated by ionospheric plasma instead of solar wind plasma.

[8] There are advantages and disadvantages to approaches outlined above. Modifying the total inner boundary density serves as a crude approximation to the actual source of ionospheric plasma, but the approach has a number of drawbacks. First, changing the inner boundary in an *ad hoc* fashion may yield accurate results, however causality is sacrificed; Is the inner boundary density high because of magnetospheric conditions, or are the conditions in the magnetosphere a result of the ionospheric boundary? Composition information of the ionosphere source is also lost. Oxygen ions make up a large fraction of the composition in the inner magnetosphere and ring current during geomagnetically active times [*Lennartsson*, 1997; *Daglis et al.*, 1999; *Fuselier et al.*, 2003]. To accurately study the impact of composition, the source population must preserve the component information, and the magnetosphere model must track the composition as it propagates. The use of empirical models to set the ion outflow rate possesses several advantages; the ionospheric source rate depends on magnetospheric conditions, the rate will correlate well with data, and it varies in a realistic manner. The drawbacks of this approach are that the mechanisms for the acceleration are ignored, and the causal chain is difficult to follow. In this study we apply a new approach to the MIC. In particular, we utilize a physics based calculation of the polar wind type outflow and put the resulting flux into an MHD model capable to tracking the outflow and its consequences.

[9] The main scientific goal of this paper is to include the plasma acceleration through the gap region between the ionosphere and magnetosphere in a self-consistent manner, and to then study the resulting effect on the space environment. First, we describe the details of our new outflow model, a field-aligned model that can obtain the solution along multiple field lines in the gap region. That model is coupled to other models (ionosphere and magnetosphere codes) through the Space Weather Modeling Framework (SWMF) [*Tóth et al.*, 2005], effectively bridging the modeling gap. We then apply our newly coupled model to the 4 May 1998 and 31 March 2001 geomagnetic storms, and examine the impact on the magnetosphere. Furthermore, the improvement in the simulated magnetospheric magnetic field, compared with that measured by various GOES satellites, is demonstrated, and the consequences of outflow to the Dst and cross polar cap potential are explored.

## 2. Model Details

[10] A significant portion of this study involved the development of a new modeling approach to magnetosphere-ionosphere coupling. A comprehensive model description is therefore appropriate. We begin by describing how the solution is obtained along a single magnetic field line, then we discuss how that solution is expanded to arrive at a full three-dimensional solution, and finally we explain the coupling between our new outflow model and the ionosphere and magnetosphere.

### 2.1. Solving a Single Field Line

[11] The first step toward obtaining a solution in the gap region is to obtain a solution to a single field line. Our work in this regard has its roots in the model of *Gombosi et al.* [1985]. The base of the field line is in the ionosphere at

**Table 1.** Chemistry in the Earth Polar Wind Model[a]

| Reaction | Reaction Rate |
|---|---|
| $O + h\nu \rightarrow O^+ + e^-$ | $I(\chi)$ |
| $He + h\nu \rightarrow He^+ + e^-$ | $3.9 \times 10^{-8}$ |
| $O + N_2 \rightarrow NO^+ + N$ | $1.2 \times 10^{-12}$ |
| $O^+ + O_2 \rightarrow O_2^+ + O$ | $2.1 \times 10^{-11}$ |
| $He^+ + O_2 \rightarrow O^+ + O + He$ | $9.7 \times 10^{-10}$ |
| $He^+ + N_2 \rightarrow N_2^+ + He$ | $5.2 \times 10^{-10}$ |
| $H^+ + O \leftrightarrow H + O^+$ | $P(H^+) = 2.5 \times 10^{-11} T^{1/2}$, $L(H^+) = 2.2 \times 10^{-11} T^{1/2}$, |

[a]The reaction rates are taken from the work of *Schunk and Nagy* [2000]. $I(\chi)$ is a calculated photoionization rate, $T$ is the temperature, and finally $P(H^+)$ and $L(H^+)$ are the production and loss rates for $H^+$ in the final reaction, respectively.

about 250 km while the top of the field line is located at a few earth radii, effectively spanning the gap. The single field line solution described in this subsection has also been used in planetary applications [see *Glocer et al.*, 2007 for details]. For the sake of a self-contained description, we repeat the description of the single line equations from *Glocer et al.* [2007].

[12] To obtain the solution in the vertical direction we solve the gyrotropic transport solution given by [*Gombosi and Nagy*, 1989]

$$\frac{\partial}{\partial t}(A\rho_i) + \frac{\partial}{\partial r}(A\rho_i u_i) = AS_i \tag{1}$$

$$\frac{\partial}{\partial t}(A\rho_i u_i) + \frac{\partial}{\partial r}\left(A\rho_i u_i^2\right) + A\frac{\partial p_i}{\partial r} = A\rho_i\left(\frac{e}{m_i}E_\parallel - g\right) + A\frac{\delta M_i}{\delta t} + Au_iS_i \tag{2}$$

$$\frac{\partial}{\partial t}\left(\frac{1}{2}A\rho_i u_i^2 + \frac{1}{\gamma_i - 1}Ap_i\right) + \frac{\partial}{\partial r}\left(\frac{1}{2}A\rho_i u_i^3 + \frac{\gamma_i}{\gamma_i - 1}Au_ip_i\right) = A\rho_i u_i\left(\frac{e}{m_i}E_\parallel - g\right) + \frac{\partial}{\partial r}\left(A\kappa_i\frac{\partial T_i}{\partial r}\right) + A\frac{\delta E_i}{\delta t} + Au_i\frac{\delta M_i}{\delta t} + \frac{1}{2}Au_i^2S_i \tag{3}$$

$$E_\parallel = -\frac{1}{en_e}\left[\frac{\partial}{\partial r}\left(p_e + \rho_e u_e^2\right) + \frac{A'}{A}\rho_e u_e^2\right] + \frac{1}{en_e}\frac{\partial}{\partial r}\left(\sum_i \frac{m_e}{m_i}\left[(u_e - u_i)S_i - \frac{\delta M_i}{\delta t}\right] + \frac{\delta M_e}{\partial t}\right). \tag{4}$$

The subscript "i" and the subscript "e" refer to the ion and electron species respectively. With regard to the other symbols, $m$ is molecular mass, $\rho$ is mass density, $u$ is velocity, $T$ is temperature, $p$ is pressure, $e$ is particle charge, $r$ is the distance along the field line, A is the cross-sectional area, $\kappa$ is the heat conductivity, $\gamma$ is the specific heat ratio, k is Boltzmann's constant, $E_\parallel$ is the ambipolar electric field, $g$ is the gravitational acceleration, $S$ is the mass production rate due to chemical reactions (see Table 1), $\frac{\delta M}{\delta t}$ is the momentum exchange rate, given by *Schunk and Nagy* [2000] as

$$\frac{\delta M_i}{\delta t} = -\sum_j \rho_i\nu_{ij}(u_i - u_j) \tag{5}$$

and $\frac{\delta E}{\delta t}$ is the energy exchange rate, given by *Schunk and Nagy* [2000] as

$$\frac{\delta E_i}{\delta t} = \sum_j \frac{\rho_i\nu_{ij}}{m_i + m_j}\left[3k(T_j - T_i) + m_j(u_i - u_j)^2\right]. \tag{6}$$

The neutrals are assumed to be at rest. The gyrotropic transport equations (continuity through efield) depend on the cross-sectional area $A$ which is inversely proportional to the magnetic field strength. Assuming a dipole we have

$$A = \alpha r^3 \tag{7}$$

where $\alpha$ is a constant, and $A' = 3\alpha\, r^2$.

[13] Equations (1) through (3) refer to the continuity, momentum, and energy equations respectively. The ambipolar electric field is given in equation (4).

[14] Unlike the ions, the electrons are not solved for using the transport equations. Rather, they are solved using charge neutrality, a steady state electron velocity assumption, and an energy equation:

$$n_e = \sum_i n_i \tag{8}$$

$$u_e = \frac{1}{n_e}\left(\sum_i n_i u_i - \frac{j}{e}\right) \tag{9}$$

$$j = j_0\frac{A_0}{A} \tag{10}$$

$$\rho_e\frac{\partial T_e}{\partial t} = (\gamma_e - 1)\frac{m_e}{kA}\frac{\partial}{\partial r}\left(A\kappa_e\frac{\partial T_e}{\partial r}\right) - \rho_e u_e\frac{\partial T_e}{\partial r} - T_e\left[S_e + \frac{\gamma_e - 1}{A}\rho_e\frac{\partial}{\partial r}(Au_e)\right] + (\gamma_e - 1)\frac{m_e}{k}\frac{\delta E_e}{\delta t} \tag{11}$$

where $j$ is the current density, and the subscript 0 represents the value taken at a reference altitude. Expression 10 enforces conservation of field aligned currents. Equation (8) represents the quasineutrality of the plasma, and substitutes for the continuity equation. Similarly, equation (9) obtains the electron velocity from the ion flux and current, and takes the place of the electron momentum equation. Finally, equation (11) obtains the electron temperature from conduction, advection, adiabatic heating, and energy transfer.

[15] Solving this system of coupled differential equations yields the density, velocity and temperature for ionospheric $O^+$, $H^+$, $He^+$ and e− along a particular field line.

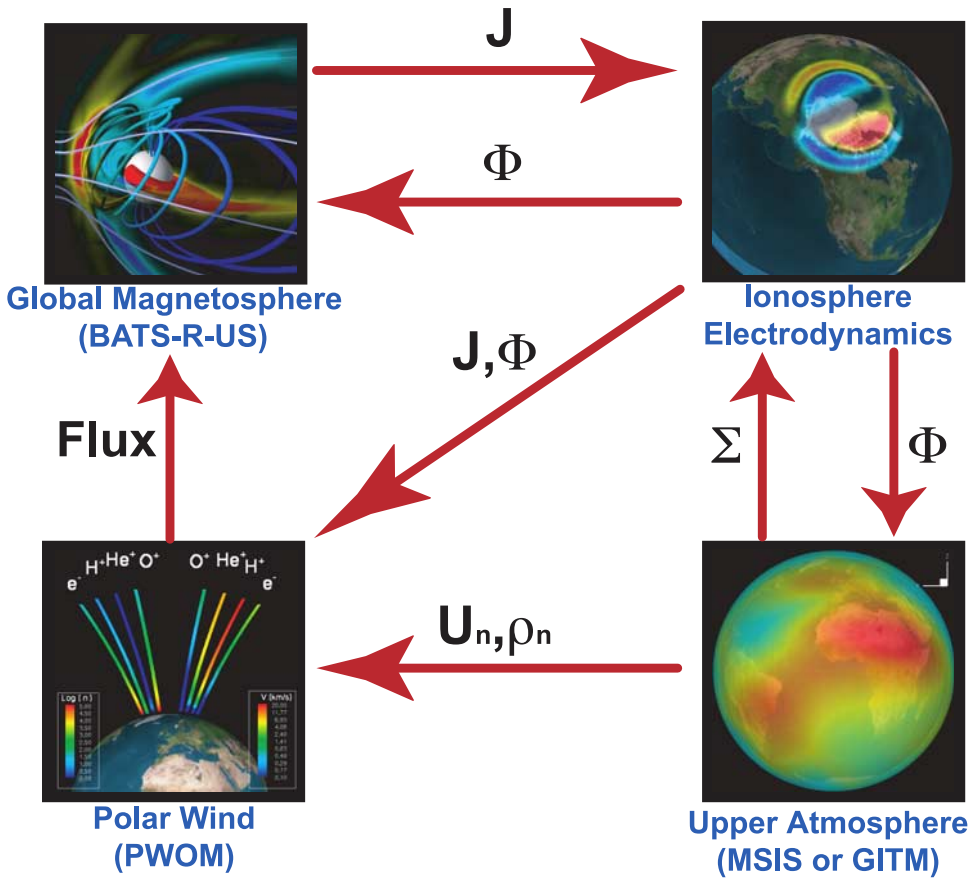


**Figure 1.** A schematic of the information exchange between components.

### 2.2. Solving Multiple Field Lines in Parallel

[16] Obtaining a vertical solution along a single field line gives only a very localized solution in the gap region. To reconstruct the full three-dimensional solution, we solve several field lines in parallel.

[17] Each field line tracked in the PWOM must be advected around the polar cap. The motion is determined through a combination of the corotation and the drift velocity given by

$$\mathbf{u}_{E\times B} = -\frac{\mathbf{E}\times\mathbf{B}}{B^2} \tag{12}$$

The electric field needed for the convection velocity is determined from the polar cap potential pattern which can either come from a file, the Weimer empirical model, or the IE component of the SWMF as detailed in the next section. Using the convection velocity is identical to using a simplified momentum equation for the horizontal solution.

[18] To speed up PWOM, we solve the field lines in parallel on multiple processors using the Message Passing Interface (MPI) library. Since there is no communication between field lines, the model exhibits ideal scaling. The only limit on the scaling is that the number of processors cannot exceed the number of field lines.

### 2.3. Incorporating the PWOM Into the SWMF

[19] We incorporate the PWOM into the Space Weather Modeling Framework (SWMF). The SWMF joins physical models of various regions into a single parallel and efficient executable [*Tóth et al.*, 2005]. Each physical region is treated as a component of the SWMF and is assigned a two letter abbreviation. The current version of the SWMF has ten components including: Solar Corona (SC), Eruptive Event Generator (EE), Inner Heliosphere (IH), Solar Energetic Particles (SP), Global Magnetosphere (GM), Inner Magnetosphere (IM), Radiation Belt (RB), Ionosphere Electrodynamics (IE), Upper Atmosphere (UA), Polar Wind (PW), Outer Heliosphere (OH), and Plasma Sphere (PS). Each component can be represented by one or more models. Moreover, the SWMF can be configured to run with any subset of components, and can be coupled both sequentially or concurrently.

[20] Figure 1 demonstrates the information flow between models used in this work, and is a schematic of the relevant couplings. We focus on the lower left portion of Figure 1 which represents the PWOM. Input from the Ionosphere Electrodynamics (IE) component is delivered in the form of polar cap potential and field aligned currents at low altitude (the method by which the IE component derives these quantities is given by *Ridley et al.* [2004]). The gradient of the potential pattern is taken to determine the electric field, which in turn is used to calculate the ionospheric convection using equation (12). The foot points of the individual field lines in the PWOM are moved accordingly. Field aligned currents from the IE component are used in equation (9) to calculate the vertical solution along each field line. It should be noted that the currents are actually

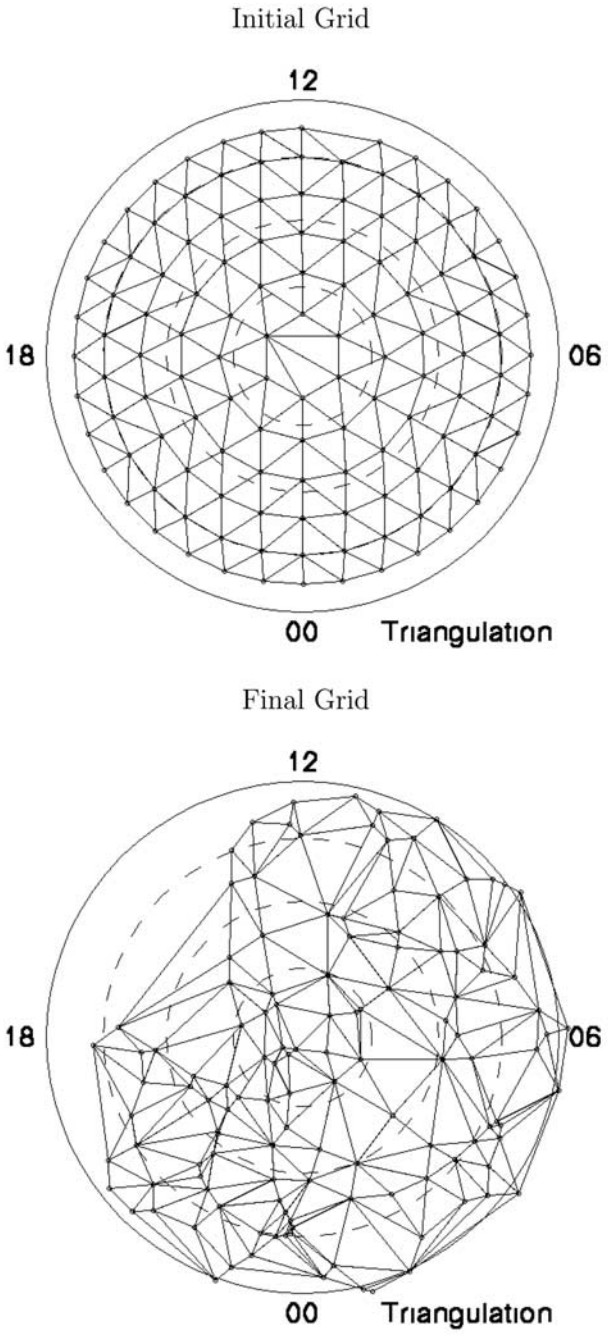


**Figure 2.** The grid triangulated onto the horizontal distribution of field lines tracked by PWOM. (top) Initial grid. (bottom) Final distribution after several hours of simulation.

originating in the GM component and then mapped to ionospheric altitudes by the IE component. We use the already mapped currents from IE for convenience.

[21] The PWOM also takes input from the Upper Atmosphere (UA) component. The neutral densities are used to calculate the chemical sources and losses according to the reactions in Table 1. The neutral winds are used to calculate the Joule heating term in the energy equation. Currently, we use the MSIS (mass spectrometer and incoherent scatter) empirical model [*Hedin*, 1983, 1987, 1991] to obtain the neutral densities and assume that the neutrals are stationary. In the future we will improve on this technique by replacing the empirical model with the physics based Global Ionosphere Thermosphere Model (GITM [*Ridley et al.*, 2006]).

[22] The resulting fluxes at the top of the PWOM are used to set the inner boundary of the Global Magnetosphere (GM) component. There are several challenges involved with incorporating the fluxes into GM. One such challenge is the differing grid. The Block-Adaptive-Tree Solar wind Roe-type Upwind Scheme, or BATS-R-US, code [*Powell et al.*, 1999; *De Zeeuw et al.*, 2000; *Gombosi et al.*, 2001], which represents the GM component, uses a block-adaptive grid while the PWOM has a totally unstructured grid in the horizontal direction. In order to interpolate between the two we need to do a Delaunay triangulation of the PWOM grid in the horizontal direction every time the components are coupled. Figure 2 shows an example of the triangulation at the beginning and end of a simulation. A grid point on the magnetosphere's inner boundary is then able to interpolate an outflow solution that corresponds to its location. Another challenge to the GM-PW coupling is putting multifluid output of PW into GM. In other words, how can we preserve the composition information when putting multifluid output into a single fluid code (BATS-R-US is usually configured for single-fluid MHD)? All the fluxes coming from the PW component then need to be combined into a single-fluid density and velocity. As an improvement over this approach, we can configure BATS-R-US for multispecies or multifluid MHD. In these cases the output from the PW component is included by either splitting the densities and using a combined velocity, or using split densities and velocities respectively. In this study, we make use of a multispecies version of BATS-R-US, where each ion species has its own continuity equation, but uses a shared momentum and energy equation.

[23] In section 3, we apply our newly coupled model to two geomagnetic storms. This initial test of our new model draws particular attention to the importance of including ionospheric outflow when examining geomagnetically active time periods.

## 3. Results: Impact of Ionospheric Outflow on Magnetospheric Composition and Magnetic Field Results

[24] A key advancement of the model presented in this study is the ability to not only simulate ion outflow, but also its broader effects on the magnetosphere. Observations have shown that during a geomagnetic storm ionospheric outflow can be the dominant contributor to the magnetosphere plasma composition [*Kistler et al.*, 2005]. It is therefore appropriate to test our newly coupled model on actual geomagnetic storms to see how the ionospheric outflow affects the magnetospheric solution. For this study we have chosen the 4 May 1998 and 31 March 2001 geomagnetic storms.

[25] For these simulations we use the SWMF configured with the PW, GM, IE, and IM components. The GM component is configured to solve the multispecies MHD equations where separate continuity equations are used for $O^+$ and $H^+$, but they share a common momentum and

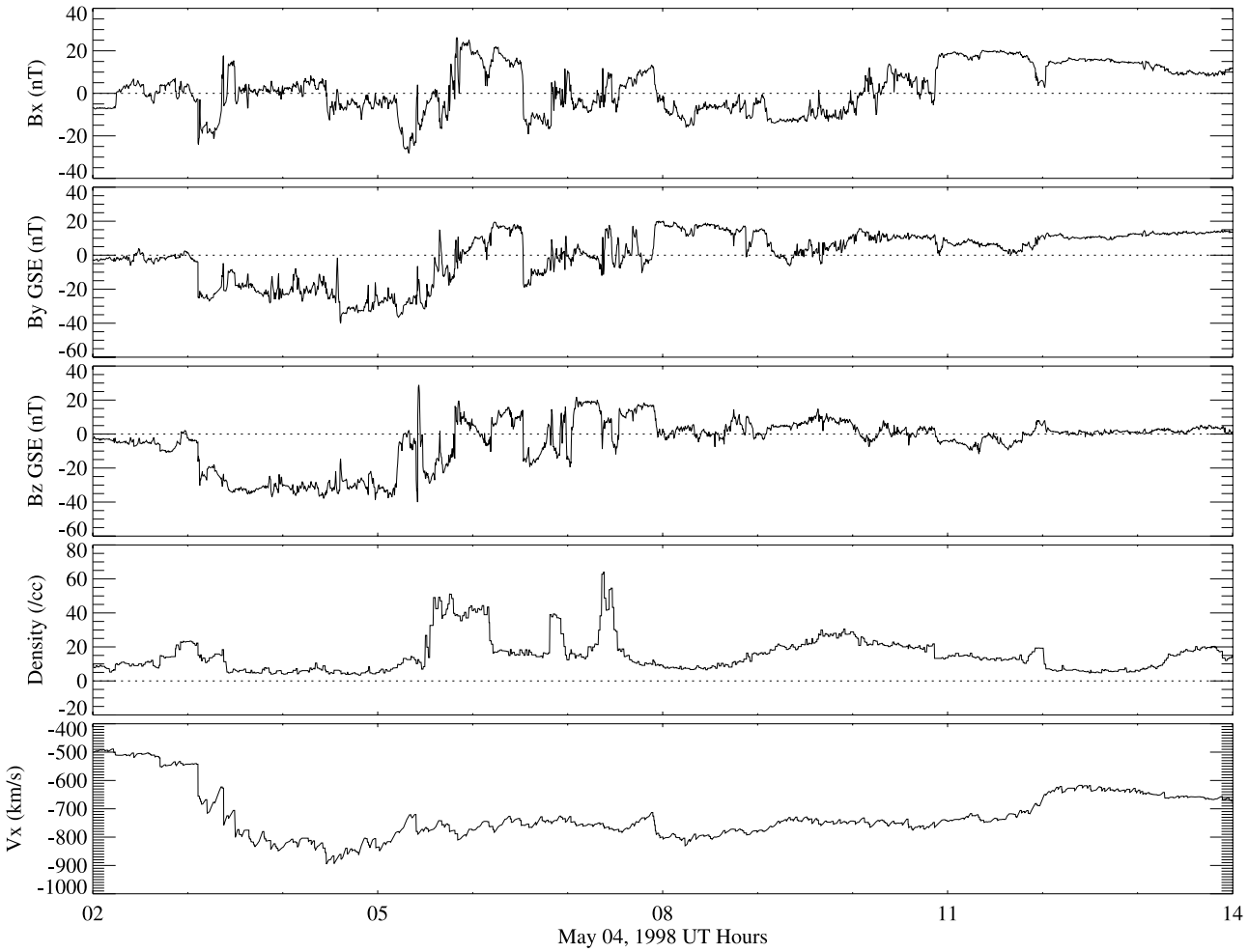


**Figure 3.** Solar wind condition used to set the upstream boundary condition for the magnetosphere for the 4 May 1998 storm.

energy equation. In this way we can track the individual species without solving the full multifluid MHD equations. Additionally, the components are coupled every ten seconds allowing for frequent exchange of information over the course of the simulation. Figures 3 and 4 show the solar wind conditions that set the upstream boundary condition for the magnetosphere in each simulation. The Kp and Ap geomagnetic indices for these events are shown in Figure 5.

[26] When calculating the outflow in the PW component we track 125 distinct field lines as they move through the polar cap. Figure 6 shows plots at representative times during the 4 May 1998 even of the out-flowing $O^+$ and $H^+$ flux at 1,500 km above the Earth's surface during the 4 May 1998 event. Also shown are the FACs and the ionospheric potential inputs at corresponding times. The three times are considered: 6:20 UT which is just after the first solar wind density spike, 7:30 UT which is during the third solar wind density spike, and 9:30 UT which is well after the density spikes. The "+" signs on the plots illustrate field line locations at the time. Close examination of the field line distribution in Figure 6 reveals a limitation of our approach. Some regions are adequately represented by field lines, while other regions are significantly underrepresented. This nonuniform distribution of field lines results despite an initially uniform coverage.

[27] Figure 6 allows us to examine the impact of the imposed magnetospheric conditions on the calculated ion outflow. This is a complicated process since our physics based model has several inputs which are all changing with time. However, a qualitative examination of the FACs together with the $O^+$ flux demonstrates a connection between the upward/downward FACs and the upward/downward $O^+$ flux. This result is in agreement with the work of *Gombosi and Nagy* [1989] who studied steady upward and downward current on the polar wind solution of a stationary magnetic field line. The impact of the ionospheric potential is harder to discern. In general, the ionospheric potential alters the convection velocity of a field line in the polar cap, thereby affecting how long the field line spends in daylight and in regions of strong FACs. The potential also impacts the outflow by altering amount of frictional heating that the ions encounter at low altitude by moving through the neutral background.

[28] Overall, the $O^+$ flux is seen to vary significantly more than the $H^+$ flux at all times considered as its magnitude runs from slight downward flow to rather strong outflow. The $H^+$ flux, by contrast, exhibits significantly less

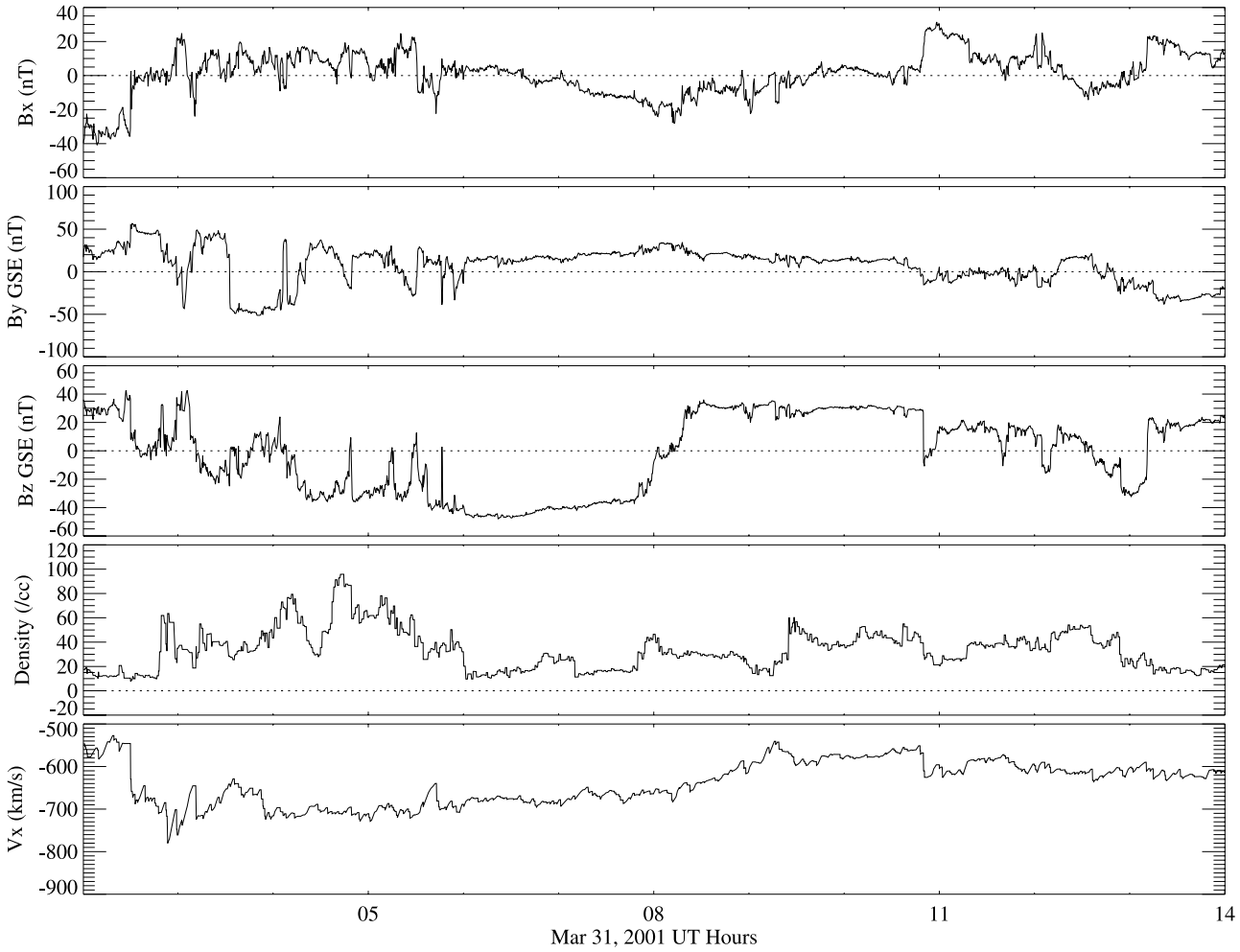


**Figure 4.** Solar wind condition used to set the upstream boundary condition for the magnetosphere for the 31 March 2001 storm.

variation across latitude and local time. Interestingly, there seems to be significantly larger $H^+$ and $O^+$ flux below 75° as compared to above 75°, a result consistent with Akebono measurements presented by *Abe et al.* [1996]. *Abe et al.* [1996] also report an $H^+$ flux that varies between $10^7$ and $10^8$ $cm^{-2}$ $s^{-1}$ at 2,000 km, a number that agrees with our simulations. Our simulated $H^+$ flux is also in the range observed by the ISIS-2 spacecraft which found a value of $2-20 \times 10^7$ $cm^{-2}$ $s^{-1}$ at 1400 km [*Hoffman and Dodson*, 1980], and for DE-1 observations which found a value of about $20 \times 10^7$ $cm^{-2}s^{-1}$ when normalized to 2000 km [*Nagai et al.*, 1984]. *Abe et al.* [1996] also examine, the

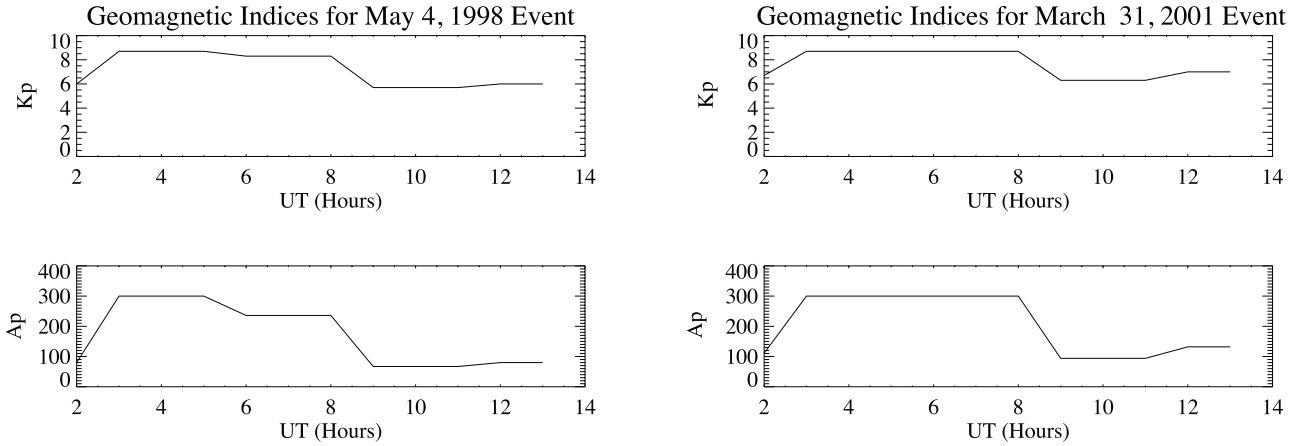


**Figure 5.** The Kp and Ap indices during the 4 May 1998 event and 31 March 2001 event.

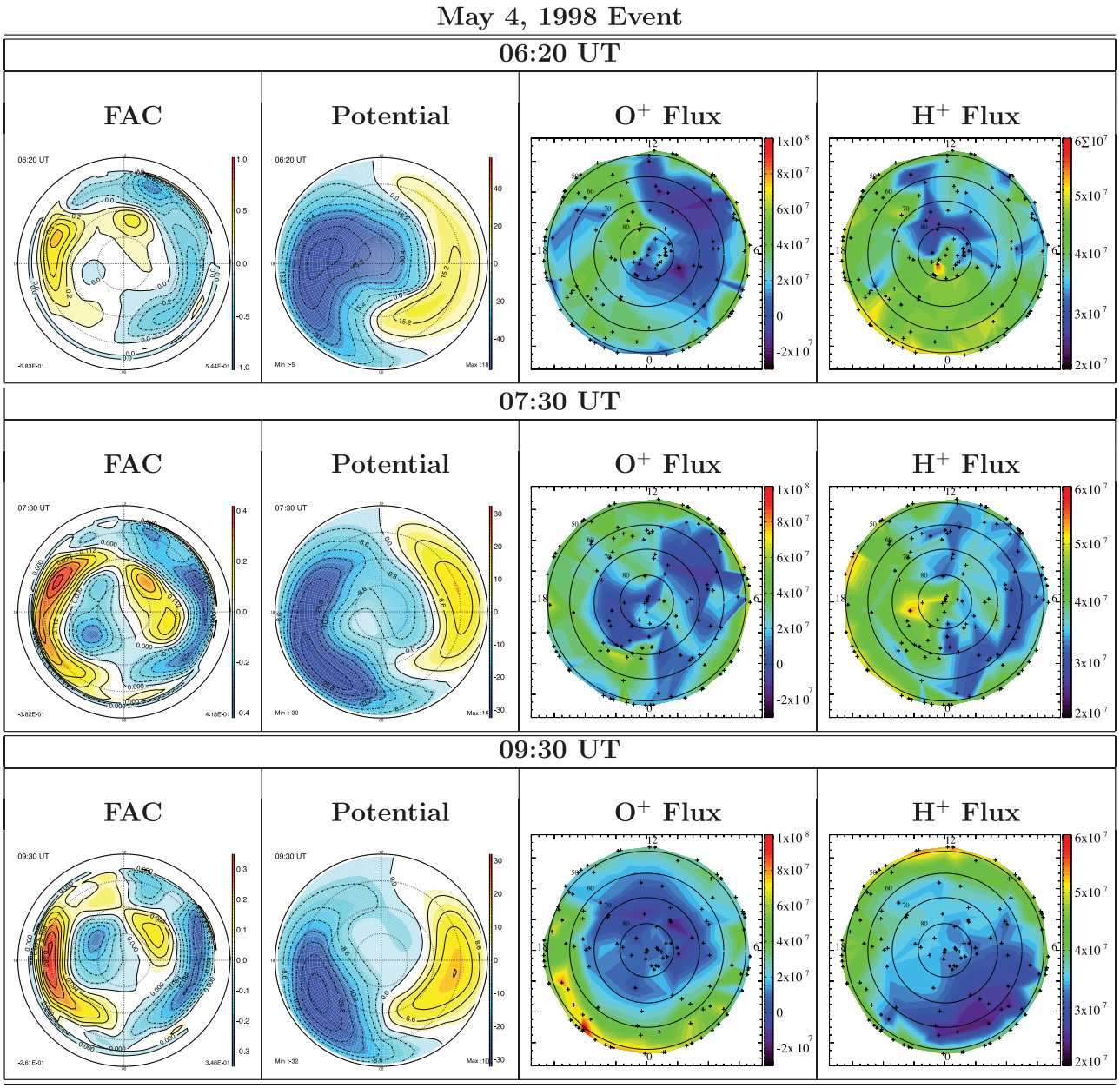


**Figure 6.** This figure shows the field-aligned current and ionospheric potential along with $O^+$ and $H^+$ flux at various times during the 4 May 1998 geomagnetic event. The field-aligned current and ionospheric potential plots are altitude slices at 150-km altitude, whereas the $O^+$ and $H^+$ fluxes are altitude slices at 1500 km. The "+" signs in the flux plots represent the foot points of magnetic field lines used in the PWOM calculation.

variation of $H^+$ and $O^+$ flux with MLT. They found that in all MLT sectors and Kp < 5 the $O^+$ flux is about a factor of 1.5–2 smaller than the $H^+$ flux, but above Kp = 5 the $O^+$ flux can equal or exceed that of $H^+$. This is consistent with what we see in our simulations. They also find that for all values of Kp the flux in the noon sector was the largest for both species. Unfortunately, we do not see this result in our simulations. A likely explanation is that our simulations deal with polar wind type outflows and do not include the physics associated with suprathermal Cusp/Cleft Ion Fountain (CIF) related outflows. As we will discuss shortly, this shortcoming of our model may be alleviated by using a better method for including the topside electron heat flux.

[29] An advantage to showing the outflow results for the 4 May 1998 event, rather than the 31 March 2001 event, is that we can directly compare with the numerical simulations of *Gardner and Schunk* [2008]. *Gardner and Schunk* [2008] use a three-dimensional model of polar wind $H^+$, $O^+$, electrons, and neutrals to study the polar wind outflow during this event. They also found significant outflow of $H^+$ and $O^+$ occurring mostly below 75° latitude, and stronger $O^+$ outflow on the dusk side. However, significant differences exist between their results and the outflow

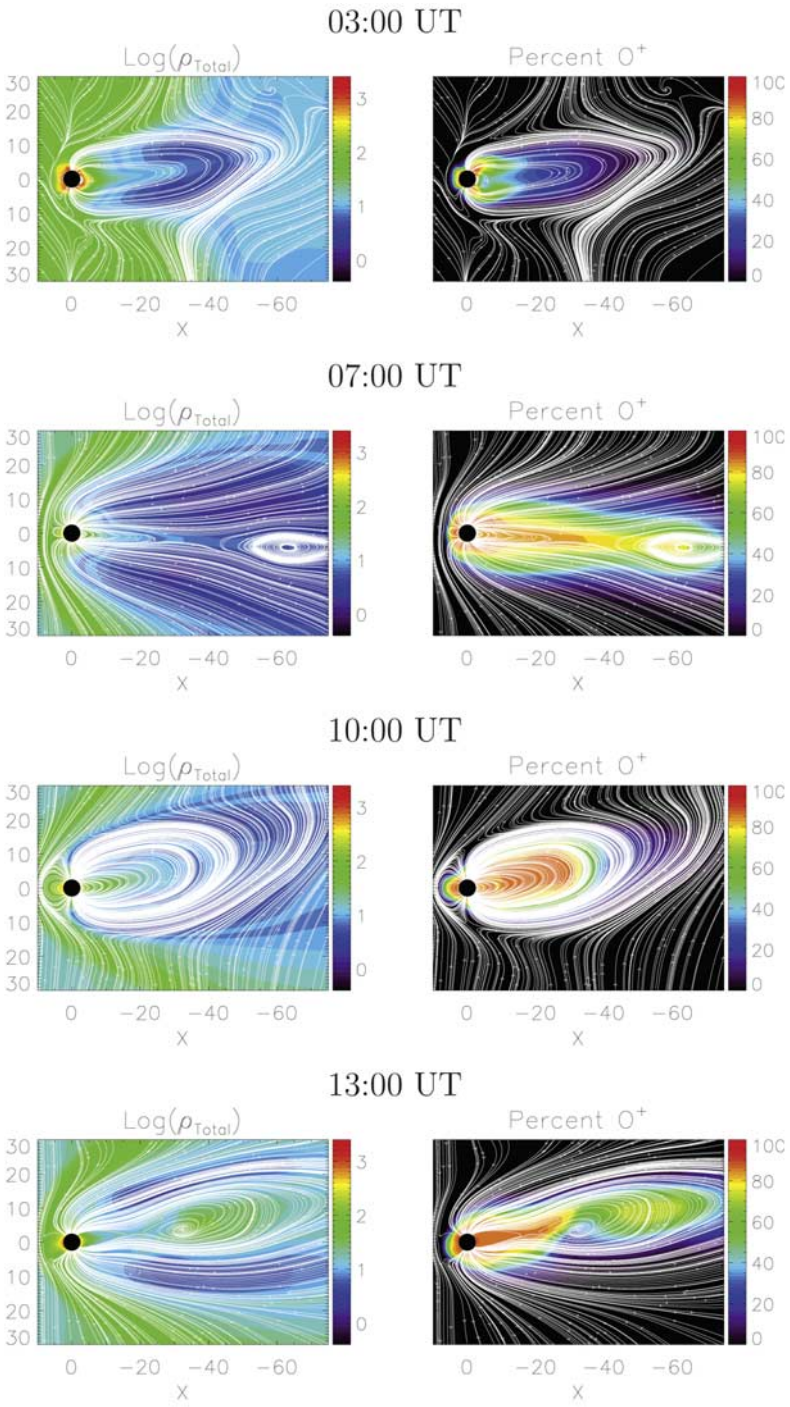


**Figure 7.** (left) Log of mass density and (right) the percentage of oxygen ions in the magnetosphere at 3, 7, 10, and 13 UT for the 31 March 2001 event. The $y = 0$ plane is shown.

results presented here. In particular, they find a flux whose peak is an order of magnitude larger than our flux. This difference is most likely due to differences in how the topside electron heat flux is included. *Gardner and Schunk* [2008] use values obtained from AMIE (Assimilative Mapping of Ionosphere Electrodynamics) [*Ridley and Kihn*, 2004] which change with time and vary over the polar cap. We simply use an average unchanging value determined by *Bekerat et al.* [2007]. In future work we will implement a more sophisticated approach, taking the heat flux from magnetosphere model. This should significantly impact the outflow magnitude and spatial distribution since the changing the heat flux will have a big impact on the electron temperature which is well correlated to outflow [*Abe et al.*, 1993]. Additionally, using a more realistic electron heat flux map may yield a more well defined auroral and cusp outflow instead of just the polar wind type outflow obtained here.

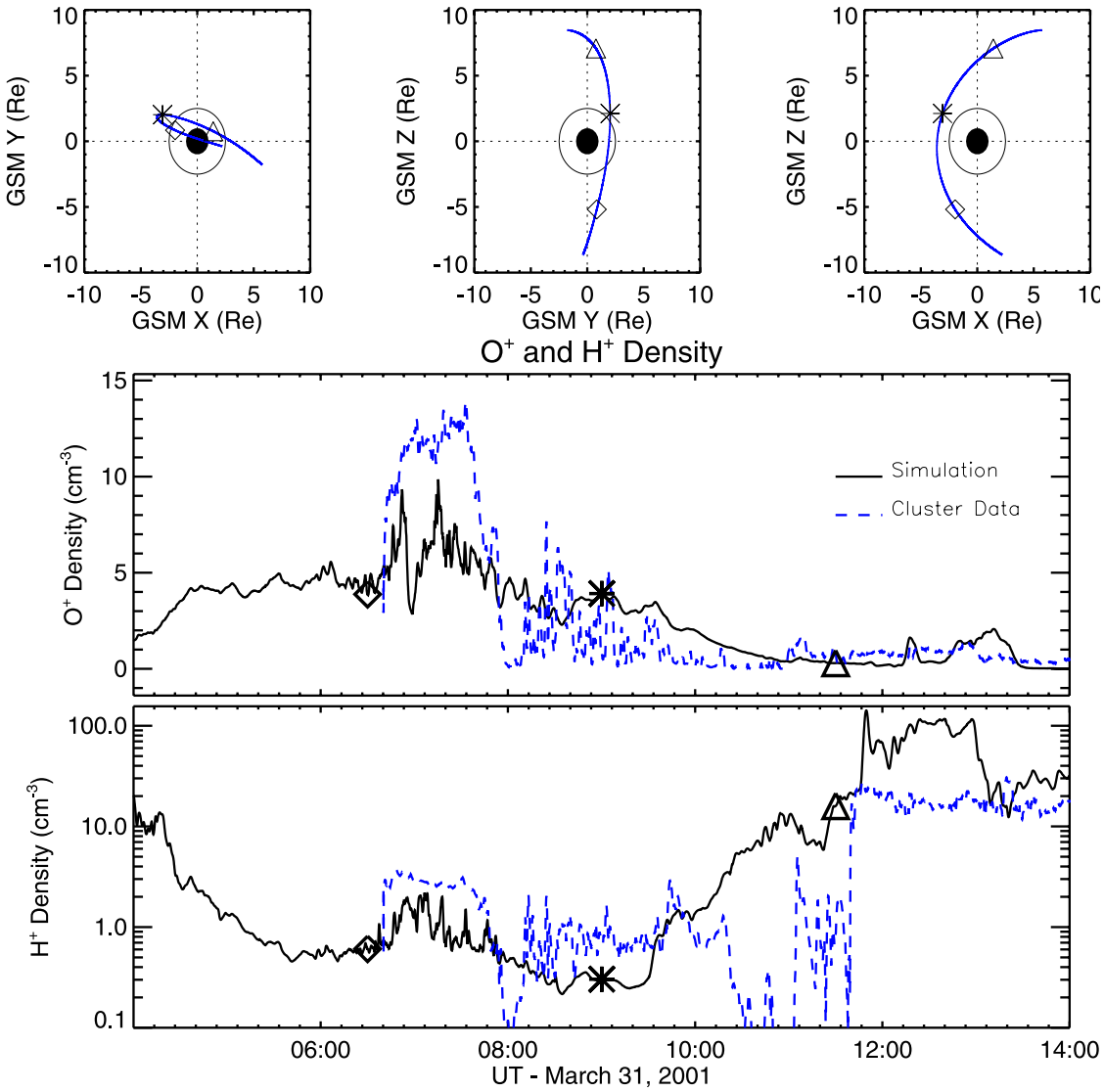


**Figure 8.** Data model comparison between the Cluster 1 satellite data (blue dashed line) and simulation (black solid line) for the 31 March 2001 event. (top) The satellite trajectory in the *Y-X*, *Z-Y*, and *Z-X* planes. (middle) Comparison of $O^+$ number density. (bottom) Comparison of $H^+$ number density. We show the bottom panel on a log linear scale because differences near the end of the comparison are large enough to make it hard to compare the first part when using a linear scale.

[30] We turn our attention now to the effect that the outflow has on the magnetosphere. The left panel of each plot in Figure 7 shows the log of the mass density along with traces of the X and Z components of the magnetic field at various points during the 31 March 2001 storm. We take advantage of the multispecies nature of the simulation and track the composition of the density in the magnetosphere, and not just the overall density. The right panel of each plot in Figure 7 illustrates the corresponding percentage of oxygen ions. The initial amount of $O^+$ in the simulation is very small, but when the storm simulation begins the magnetosphere begins to fill with $O^+$. Eventually $O^+$ composes a large fraction of the magnetosphere population. The progression is shown in four panels. After one hour of simulation time (3 UT), we see the $O^+$ beginning to making its way into the magnetosphere. Five hours into the simulation (7 UT) there is a strongly negative solar wind Bz and an *X* line forms between 30 and 40 Earth Radii down tail; $O^+$ is now quite prevalent. After eight hours (10 UT), the solar wind Bz becomes strongly positive, increasing the closed field-line region to higher latitude, and more effectually trapping the out-flowing ionospheric plasma. The last panel shows the configuration near the end of the simulation where the upstream Bz has again turned negative. To save space, we do not show the results for the 4 May 1998 event.

[31] The plots in Figure 7 predict a significant amount of $O^+$ in the magnetosphere. To verify this aspect of the simulation, we compare our model results directly with Cluster s/c 1 satellite data. The choice of Cluster s/c 1 is arbitrary since the spacing between satellites is much less then a grid cell size. The Cluster Ion Spectrometry (CIS) experiment on-board the Cluster satellite is capable of measuring the distribution of magnetospheric $H^+$, $He^+$, $He^{++}$, and $O^+$ ions from thermal energies to about 40 keV/e

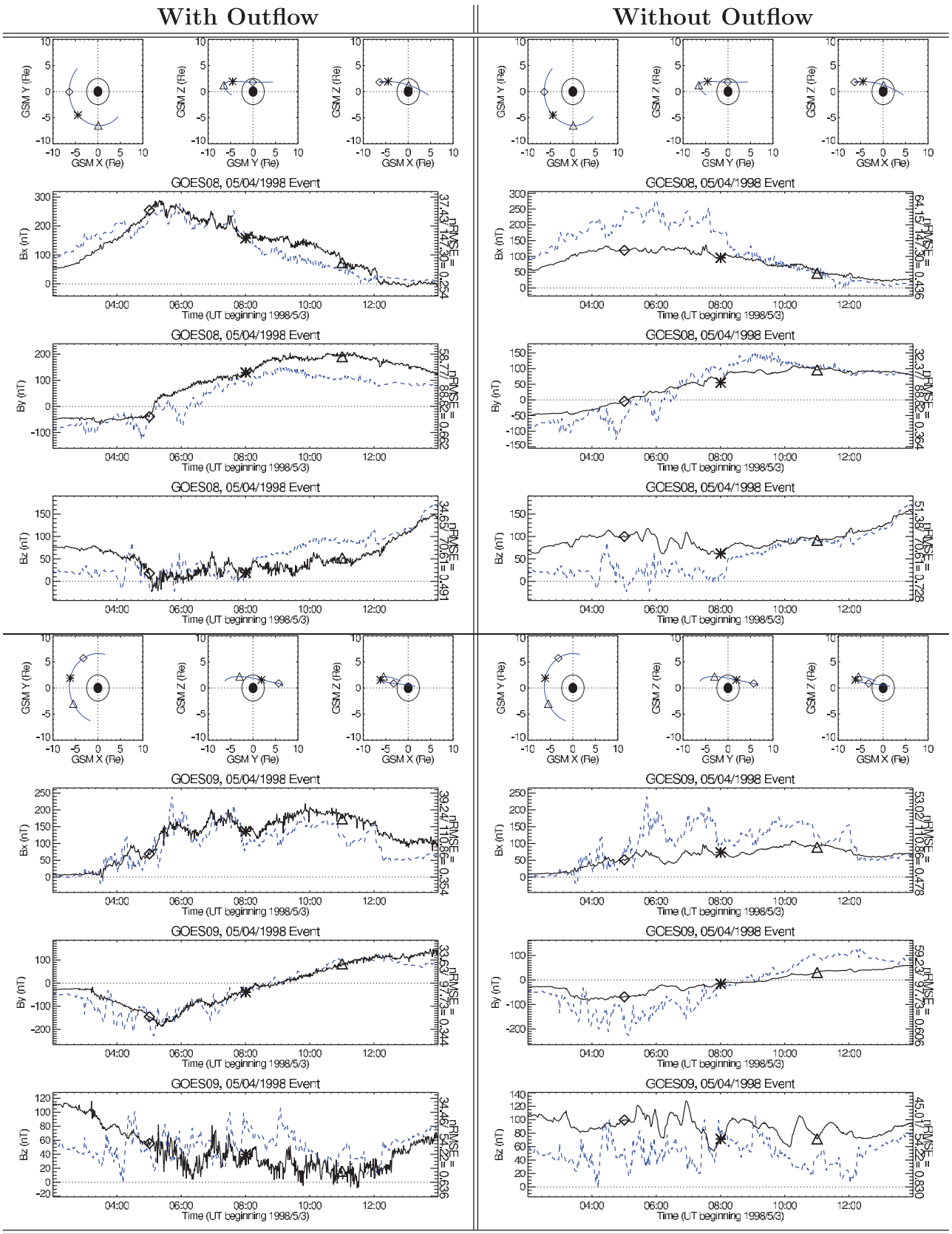


**Figure 9.** Data model comparisons of magnetic field from Goes 08 and Goes 09 with the MHD magnetic field calculated by BATS-R-US for the 4 May 1998 event. The data are in blue, and the simulations are in black.

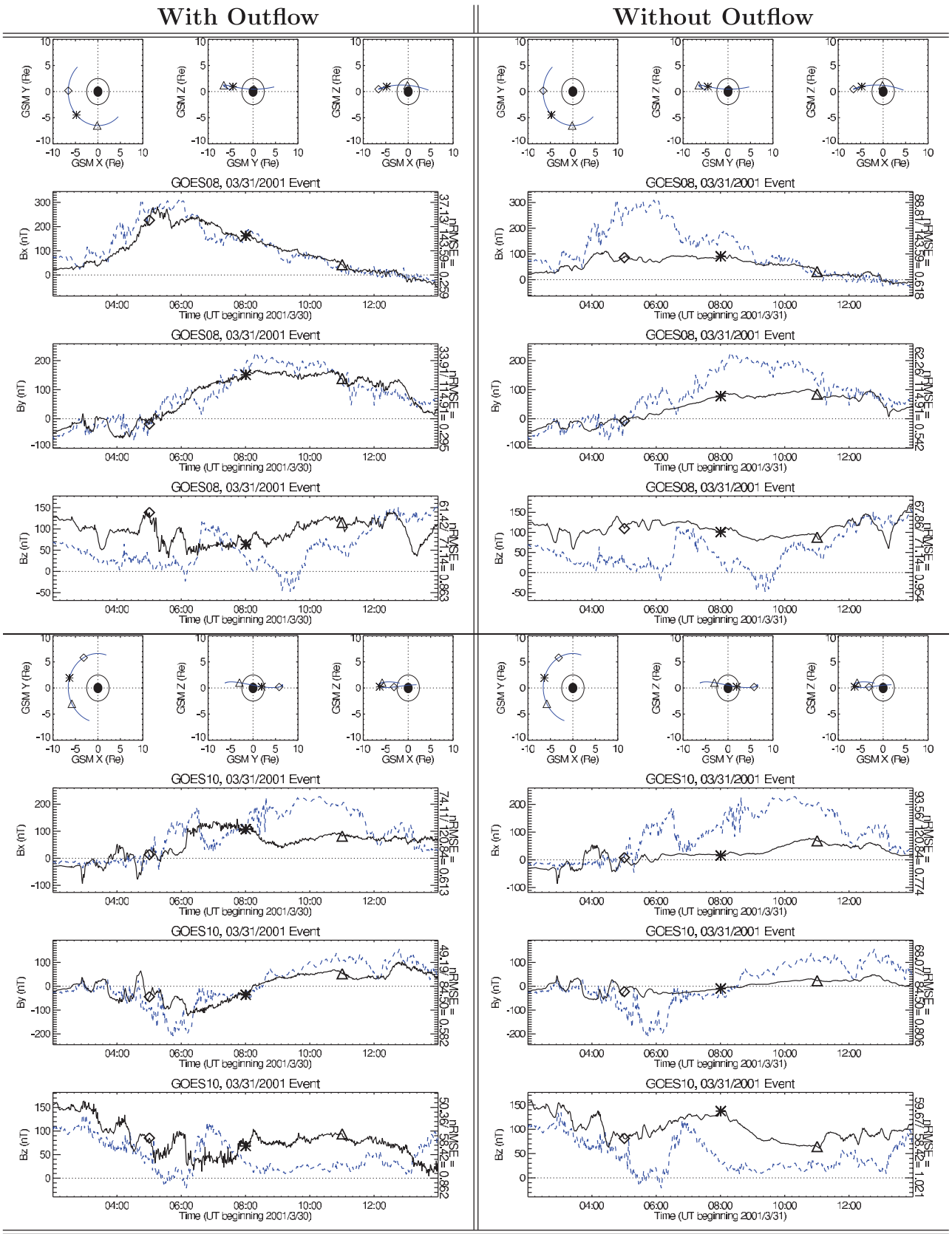


**Figure 10.** Data model comparisons of magnetic field from Goes 08 and Goes 10 with the MHD magnetic field calculated by BATS-R-US for the 31 March 2001 event. The data are in blue, and the simulations are in black.

**Table 2.** Summary of the Root Mean Square (RMS) Error Between Data at Various GOES Satellites and Simulated Output at Those Locations

| | | RMS Error in $\|B\|$ | | RMS Error in Elevation Angle | |
|---|---|---|---|---|---|
| Event | Satellite | With Outflow | Without Outflow | With Outflow | Without Outflow |
| 4 May 1998 | GOES 08 | 0.243 | 0.260 | 0.649 | 0.808 |
| | GOES 09 | 0.225 | 0.317 | 0.755 | 1.163 |
| 31 March 2001 | GOES 08 | 0.179 | 0.363 | 0.681 | 1.084 |
| | GOES 10 | 0.406 | 0.472 | 0.775 | 1.161 |

[*Rème et al.*, 2001]. In Figure 8, we show the Cluster reference satellite's trajectory during the 31 March 2001 event, and direct comparisons between the measured ion number densities, from the CIS experiment, and values extracted from the simulation along the trajectory. The measured $O^+$ density compares well with the simulation result. However, the simulated $H^+$ density, which compares well at first, deviates significantly from the measured density after about 10 UT. Because there are only Cluster data available after 2001, we do not carry out a similar comparison for the 4 May 1998 event.

[32] The difference between the simulated and observed $H^+$ density, seen in Figure 8, has two major causes: (1) At 12 UT Cluster measures an increase in $He^{++}$, and magnetic signatures, indicating that the satellites is in the sheath region. The upstream solar wind conditions during this time period range from about 20 to 50 $cm^{-3}$ (see Figure 4). Densities in the magnetosheath should be at least as large and most likely larger as the solar wind is compressed. While Cluster does see a jump in $H^+$ density at 12 UT, it never measures a density larger than 20 $cm^{-3}$. This indicates that Cluster may not be measuring the full distribution function at this time. Indeed, when Cluster enters certain magnetosheath and solar wind modes, as it does at 12 UT, then the satellites does not measure the entire distribution function according to the "Cluster Active Archive: Interface Control Document for CIS" (available at http://caa.estec.esa.int/caa). This observational mode, and its associated consequences, accounts for differences in $H^+$ after 12 UT. (2) The simulated Cluster satellite encounters the backside of the magnetosheath two hours earlier (10 UT) than the actual satellite (12 UT). As a result, the $H^+$ density begins to increase earlier than it should. Note, we do not carry out a similar comparison for the simulation without outflow since composition information is simply unavailable.

[33] In order to quantify the impact of ionospheric outflow on the magnetosphere we compare the solution at specific satellite locations with the corresponding data. In particular, we examine magnetic field data from the GOES satellites compared with simulation output. Simulations with no ion outflow are included as a control case. For the 4 May 1998 event, direct data model comparisons are shown for GOES 08 and GOES 09 in Figure 9. Direct comparisons for the 31 March 1998 event, using GOES 08 and GOES 10, are shown in Figure 10. At first sight it is clear that the agreement between the data and model improves significantly when the ionospheric outflow is included. Moreover, when the root mean square (RMS) errors are compared, the error is reduced by as much as a factor of two when outflow is included. The RMS error for each magnetic field component is shown in Figures 9 and 10 to the right of the plots. We also summarize the RMS errors in the field magnitude and elevation angle in Table 2. It is interesting to note that while the error in both the elevation and field magnitude are reduced when outflow is included, the reduction in RMS error is consistently larger for the elevation angle. This suggests that the outflow has less effect on the field strength, and more on the field direction.

[34] There are several contributing factors, both physical and numerical, to the improved agreement between the GOES data and the simulations when outflow is included. When outflow is included the total density in the magnetosphere is increased. As a result there is an increased source population for the ring current. The ring current model, represented by the Rice Convection Model (RCM), energizes the plasma and increases the pressure and temperature which is then fed back to the global magnetosphere. The result is an increased plasma beta which makes the plasma more responsive to the solar wind driver. The increased density also decreases the Alfvén speed which in turn reduces the amount of numerical diffusion. Additionally, *Shay and Swisdak* [2004] found that including oxygen ions can lead to lower reconnection rates. In our simulations the reduced Alfvén speed resulting from the increased mass density can reduce the reconnection rate changing the result in the tail. These effects, working in concert, improve the data model comparison.

[35] We can test the statement in the previous paragraph, that the ring current is strengthened when outflow is included, by examining the simulated Dst index; Here we treat the Dst index as proxy for ring current strength. Figure 11 shows the simulated Dst index when ionospheric outflow is included, and when it is not. The panel on the left shows the 4 May 1998 event and panel on the right shows the 31 March 2001 event. Simulated Dst is determined by using the Biot-Savart formula to determine the field at the Earth's center due to the magnetospheric currents. The actual Dst index is overplotted as a reference. In both cases, it is clear that the simulations with outflow have much stronger simulated Dst indices. In fact, for the 4 May 1998 event with outflow the simulated Dst to low (compared to the measured Dst) when outflow is included whereas it is not low enough when no outflow is included. The simulated Dst for the 31 March 2001 event (with outflow) does a better job of matching measured Dst.

[36] Clearly, when the magnetosphere is modeled with ion outflow and ring current, the comparison with the magnetic field measured by GOES satellites is better than with only ring current. The next question is: Can we neglect

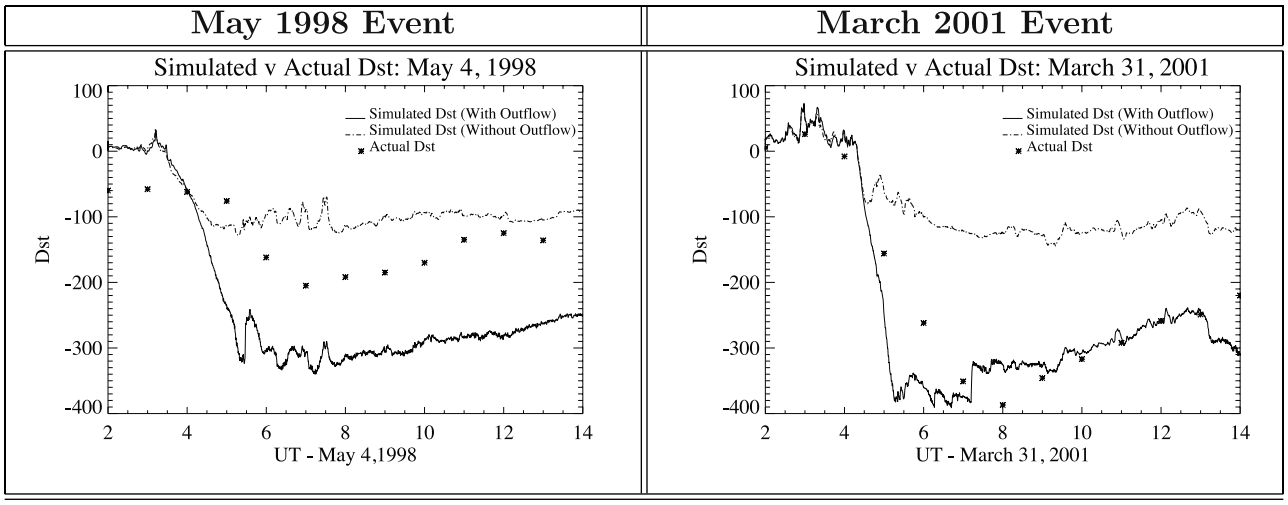


**Figure 11.** A comparison of the simulated Dst with and without outflow with the measured Dst.

any part of this system and still obtain these results? To answer the question, we repeated the simulation with only the GM and PW components and the ring current (IM component) switched off. The resulting comparisons are worse than when all components are included. Therefore it appears that to model the magnetosphere, or at least the magnetic field at geosynchronous orbit and the Dst, the contributions from the ring current and the ion outflow must be included.

[37] The outflow also reduces the Cross Polar Cap Potential (CPCP). Figure 12 shows the simulated CPCP when ionospheric outflow is included, and when it is not. The panel on the left shows the 4 May 1998 event and panel on the right shows the 31 March 2001 event. The CPCP derived by AMIE (Assimilative Mapping of Ionosphere Electrodynamics [*Ridley and Kihn*, 2004]) is included as a reference. In both cases, the outflow leads to lower CPCP. The changing polar cap potential can further alter not only the solution in the magnetosphere, but it can provide feedback to the calculated outflow as well. It is not clear that the decrease in CPCP, which has also been found in other numerical studies [see *Winglee et al.*, 2002, for instance], is an improvement. Indeed, it appears that the simulated CPCP compares better, at times, with the AMIE derived quantity if we do not include outflow. However, both simulations qualitatively compare well with the AMIE derived CPCP. This interesting conundrum of how the outflow can so dramatically improve the solution in the magnetosphere, while at the same time reducing the quality of the compared CPCP certainly warrants further study.

## 4. Conclusion and Discussion

[38] This study outlines a new method for studying ionospheric outflow and its effect on the magnetosphere. We developed the PWOM, a new model for ion outflow, and incorporated it into the SWMF. The coupled model allows us to examine outflow as a part of the space environment system. By treating the outflow as part of a system, we can examine its broader influence on the

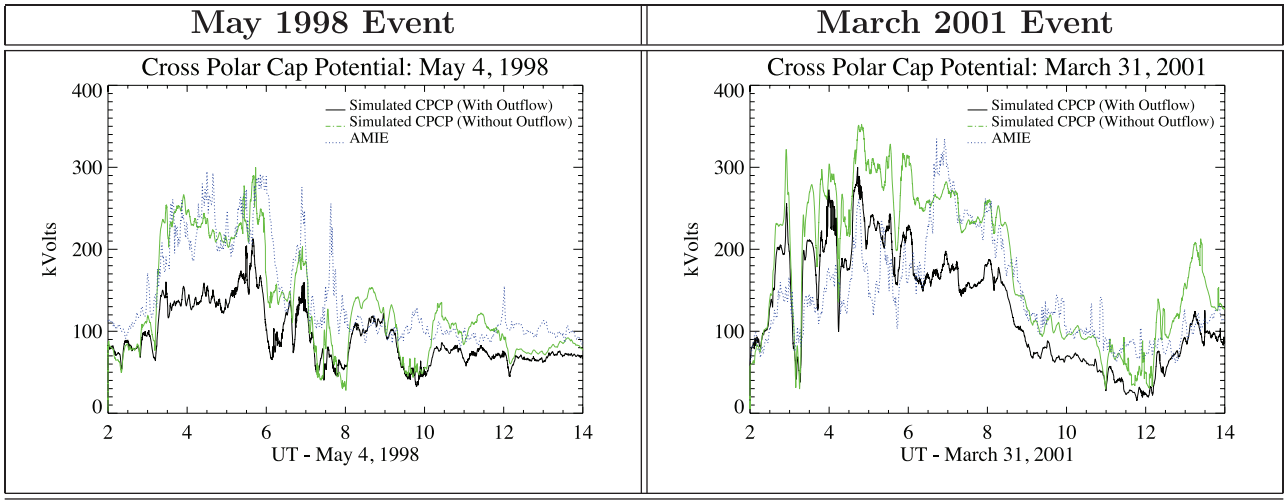


**Figure 12.** A comparison of the simulated northern cross-polar cap potential (CPCP) with and without outflow with the AMIE [*Ridley and Kihn*, 2004] derived CPCP.

magnetosphere. The simulations carried out in this section demonstrate the importance of including ion outflow in magnetospheric simulations.

[39] The simulations of the 4 May 1998 and 31 March 2003 storms clearly illustrate the necessity of including the ionospheric contribution to the magnetosphere. When comparing GOES data to simulations with and without ion outflow, we find that the RMS error is significantly reduced when including outflow. The explanation for the improvement, provided in the previous section, relies on the energization of plasma of ionospheric origin through interaction with the ring current and the modification of the Alfvén speed in the magnetosphere. Indeed, a comparison of the simulated Dst indices demonstrate the strong influence that the outflow has on the ring current strength. As an experiment, the simulation was repeated with the IM component turned off. The comparison with data was much worse than when the ring current was not included. It is therefore clear that both outflow and ring current are needed to accurately model the magnetosphere during a storm, and if any cog in that system is neglected the final comparison with data is weak.

[40] The importance of including ionospheric outflow to the storm time ring current was a hypothesis of *Shelley et al.* [1972] and *Moore et al.* [2001]. Indeed, the data show that the energy density ratio of $O^+$ to $H^+$ increases with the magnitude of the Dst index [*Nosé et al.*, 2005]. Our results confirm the hypothesis and are in accord with the data. Furthermore, the outflow is shown to not just strengthen the ring current during storm time, but change the magnetospheric magnetic field to significantly impact the comparison with satellite observations.

[41] We also found that the inclusion of ionospheric outflow can lead to a reduction of the CPCP during geomagnetic storms. This result is consistent with the study of *Winglee et al.* [2002]. In that study *Winglee et al.* [2002] also found that including ionospheric outflow reduces the CPCP by means of mass loading the magnetosphere which in turn affects the momentum transfer between the solar wind and the magnetosphere. That mechanism is also at work in this study, but is probably not the sole source of the reduction in CPCP. The improved calculation of magnetospheric magnetic field, as compared with data, also yields a better calculation of the field aligned currents. Moreover, the largest mass increase naturally occurs near the inner boundary of the BATS-R-US model where the outflow is specified. This affects the calculation of the current near the inner boundary that directly affects the ionospheric potential through an Ohm's law type calculation, and by changing the precipitation which by extension alters the height integrated conductivity in the ionosphere. The relative contribution of these effects is not immediately obvious and will therefore be left to future work.

[42] Another striking feature of the simulation is the relatively high concentration of $O^+$ in the magnetosphere. Work by *Nosé et al.* [2005] showed that the energy density ratio between oxygen and hydrogen ions can get quite large during storms. *Kistler et al.* [2005] found that the contribution of $O^+$ to the total number density and pressure during substorms increases, creating a $O^+$:$H^+$ ratio as high as 10:1. While such large fractions exist, it is not clear that the large percentage of $O^+$ that persists throughout our simulations and visible far down the tail is reasonable. To assess this situation we directly compared the 31 March 2001 event simulated $O^+$ densities to those measured by the Cluster satellite. We found extremely good agreement which indicates that the predicted amount of $O^+$ is comparable to the available data. More studies are needed to verify simulated composition at various points in the magnetosphere. Future studies should include more storms and additional direct comparisons to composition data.

[43] The results highlighted in this paper demonstrate the value of treating the space environment as a coupled system rather than a group of independent domains. The effect that the outflow has on the ring current, Alfvén speed, and magnetospheric composition are all things that could not be studied in the same complete manner by using independent models of each domain. By continued improvements in the underlying models and the coupling between them, these types of studies can tackle more intricate problems.

[44] The work presented in this paper is a promising first step, but there is still much to do. More storm simulations are needed to strengthen the conclusion that the inclusion of ion outflow is vital to modeling geomagnetic storms. Additional improvements to the model are also needed. For instance, future work will utilize a true multifluid MHD model of the magnetosphere, where each fluid has its own continuity, momentum and energy equation rather than the multispecies (only separate continuity equations) approach taken in this study. Additionally, validation of the PWOM outflow will be undertaken in future work. Despite the work that remains to be done, the impact of outflow on the magnetospheric solutions found in this study is definitely significant.

[45] **Acknowledgments.** The Dst index is provided by World Data Center for Geomagnetism, Kyoto, and the Dst observatories (Kakioka, Honolulu, San Juan, Hermanus, and Alibag). We would also like to thank National Space Science Data Center for providing the ACE and GOES data: ACE MAG instrument (N.F. Ness), SWEPAM instrument (D. McComas), and GOES magnetometer (H. Singer). We would also like to acknowledge the CIS instrument team and ESA Cluster Active Archive for providing the Cluster data.

[46] Zuyin Pu thanks Jichun Zhang and another reviewer for their assistance in evaluating this paper.

## References

Abe, T., B. A. Whalen, A. W. Yau, S. Watanabe, E. Sagawa, and K. I. Oyama (1993), Altitude profile of the polar wind velocity and its relationship to ionospheric conditions, *Geophys. Res. Lett.*, *20*, 2825–2828.

Abe, T., S. Watanabe, B. A. Whalen, A. W. Yau, and E. Sagawa (1996), Observations of polar wind and thermal ion outflow by akebono/sms, *J. Geomagn. Geoelectr.*, *48*, 319–325.

Abe, T., A. W. Yau, S. Watanabe, M. Yamada, and E. Sagawa (2004), Long-term variation of the polar wind velocity and its implication for the ion acceleration process: Akebono/suprathermal ion mass spectrometer observations, *J. Geophys. Res.*, *109*, A09305, doi:10.1029/2003JA010223.

Bekerat, H. A., R. W. Schunk, and L. Scherliess (2007), Estimation of the high-latitude topside electron heat flux using DMSP plasma density measurements, *J. Atmos. Sol.-Terr. Phys.*, *69*, 1029–1048, doi:10.1016/j.jastp.2007.03.015.

Cannata, R. W., and T. I. Gombosi (1989), Modeling the solar cycle dependence of quiet-time ion upwelling at high geomagnetic latitudes, *Geophys. Res. Lett.*, *16*, 1141–1144.

Daglis, I. A., R. M. Thorne, W. Baumjohann, and S. Orsini (1999), The terrestrial ring current: Origin, formation, and decay, *Rev. Geophys.*, *37*, 407, doi:10.1029/1999RG900009.

De Zeeuw, D. L., T. I. Gombosi, C. P. T. Groth, K. G. Powell, and Q. F. Stout (2000), An adaptive MHD method for global space weather simulations, *IEEE Trans. Plasma Sci.*, *28*, 1956–1965.

Fuselier, S. A., S. B. Mende, T. E. Moore, H. U. Frey, S. M. Petrinec, E. S. Claflin, and M. R. Collier (2003), Cusp dynamics and ionospheric outflow, *Space Sci. Rev.*, *109*, 285–312, doi:10.1023/B:SPAC.0000007522.71147.b3.

Gagne, J. (2005), Implementation of ionospheric outflow in the lfm global mhd magnetospheric simulation, Ph.D. thesis, Dartmouth College.

Gardner, L. C., and R. W. Schunk (2008), Pulsating of the generalized ion and neutral polar winds, *J. Atmos. Sol.-Terr. Phys.*, *70*, 1408–1418, doi:10.1016/j.jastp.2008.03.019.

Glocer, A., T. I. Gombosi, G. Toth, K. C. Hansen, A. J. Ridley, and A. Nagy (2007), Polar wind outflow model: Saturn results, *J. Geophys. Res.*, *112*, A01304, doi:10.1029/2006JA011755.

Gombosi, T. I., and A. Nagy (1989), Time-dependent modeling of field aligned current-generated ion transients in the polar wind, *J. Geophys. Res.*, *94*, 359–369.

Gombosi, T. I., T. E. Cravens, and A. F. Nagy (1985), A time-dependent theoretical model of the polar wind: Preliminary results, *Geophys. Res. Lett.*, *12*, 167–170.

Gombosi, T. I., L. K. Kerr, A. F. Nagy, and R. W. Cannata (1991), Helium in the polar wind, *Adv. Space Res.*, *12*(6), 183–186.

Gombosi, T. I., G. Tóth, D. L. De Zeeuw, K. C. Hansen, K. Kabin, and K. G. Powell (2001), Semi-relativistic magnetohydrodynamics and physics-based convergence acceleration, *J. Comput. Phys.*, *177*, 176–205.

Hedin, A. (1983), A revised thermospheric model based on mass spectometer and incoherent scatter data: MSIS-83, *J. Geophys. Res.*, *88*, 10,170–10,188.

Hedin, A. (1987), MSIS-86 thermospheric model, *J. Geophys. Res.*, *92*, 4649–4662.

Hedin, A. (1991), Extension of the MSIS thermosphere model into the middle and lower atmosphere, *J. Geophys. Res.*, *96*, 1159–1172.

Hoffman, J. H., and W. H. Dodson (1980), Light ion concentrations and fluxes in the polar regions during magnetically quiet times, *J. Geophys. Res.*, *85*, 626–632.

Huddleston, M. M., C. R. Chappell, D. C. Delcourt, T. E. Moore, B. L. Giles, and M. O. Chandler (2005), An examination of the process and magnitude of ionospheric plasma supply to the magnetosphere, *J. Geophys. Res.*, *110*, A12202, doi:10.1029/2004JA010401.

Kistler, L. M., et al. (2005), Contribution of nonadiabatic ions to the cross-tail current in an $O^+$ dominated thin current sheet, *J. Geophys. Res.*, *110*, A06213, doi:10.1029/2004JA010653.

Lennartsson, O. W. (1997), ISEE Ion Composition Data with Implications for Solar Wind Entry into Earth's Magnetotail, *Space Sci. Rev.*, *80*, 305–323.

Lotko, W. (2007), The magnetosphere ionosphere system from the perspective of plasma circulation: A tutorial, *J. Atmos. Sol.-Terr. Phys.*, *69*, 191–211, doi:10.1016/j.jastp.2006.08.011.

Lyon, J., J. Fedder, and C. Mobarry (2004), The Lyon-Fedder-Mobarry (LFM) global MHD magnetospheric simulation code, *J. Atmos. Sol.-Terr. Phys.*, *66*, 1333.

Moore, T. E. (1984), Superthermal ionospheric outflows, *Rev. Geophys.*, *22*, 264–274.

Moore, T. E., M. O. Chandler, M.-C. Fok, B. L. Giles, D. C. Delcourt, J. L. Horwitz, and C. J. Pollock (2001), Ring currents and internal plasma sources, *Space Sci. Rev.*, *95*, 555–568.

Moore, T. E., M.-C. Fok, D. C. Delcourt, S. P. Slinker, and J. A. Fedder (2007), Global aspects of solar wind ionosphere interactions, *J. Atmos. Sol.-Terr. Phys.*, *69*, 265–278, doi:10.1016/j.jastp.2006.08.009.

Nagai, T., J. H. Waite Jr., J. L. Green, C. R. Chappell, R. C. Olsen, and R. H. Comfort (1984), First measurements of supersonic polar wind in the polar magnetosphere, *Geophys. Res. Lett.*, *11*, 669–672.

Nosé, M., R. W. McEntire, and S. P. Christon (2003), Change of the plasma sheet ion composition during magnetic storm development observed by the Geotail spacecraft, *J. Geophys. Res.*, *108*(A5), 1201, doi:10.1029/2002JA009660.

Nosé, M., S. Taguchi, K. Hosokawa, S. P. Christon, R. W. McEntire, T. E. Moore, and M. R. Collier (2005), Overwhelming $O^+$ contribution to the plasma sheet energy density during the October 2003 superstorm: Geotail/EPIC and IMAGE/LENA observations, *J. Geophys. Res.*, *110*, A09S24, doi:10.1029/2004JA010930.

Powell, K., P. Roe, T. Linde, T. Gombosi, and D. L. De Zeeuw (1999), A solution-adaptive upwind scheme for ideal magnetohydrodynamics, *J. Comp. Physiol.*, *154*, 284–309.

Pulkkinen, T. I., N. Yu. Ganushkina, D. N. Baker, N. E. Turner, J. F. Fennell, J. Roeder, T. A. Fritz, M. Grande, B. Kellett, and G. Kettman (2001), Ring current ion composition during solar minimum and rising solar activity: Polar/CAMMICE/MICS results, *J. Geophys. Res.*, *106*, 19,131–19,147.

Rème, H., et al. (2001), First multispacecraft ion measurements in and near the Earth's magnetosphere with the identical Cluster ion spectrometry (CIS) experiment, *Ann. Geophys.*, *19*, 1303–1354.

Ridley, A. J., and E. A. Kihn (2004), Polar cap index comparisons with amie cross polar cap potential, electric field, and polar cap area, *Geophys. Res. Lett.*, *31*, L07801, doi:10.1029/2003GL019113.

Ridley, A., T. Gombosi, and D. Dezeeuw (2004), Ionospheric control of the magnetosphere: Conductance, *Ann. Geophys.*, *22*, 567–584.

Ridley, A. J., Y. Deng, and G. Tóth (2006), The global ionosphere thermosphere model, *J. Atmos. Sol.-Terr. Phys.*, *68*, 839–864, doi:10.1016/j.jastp.2006.01.008.

Schunk, R. W., and A. F. Nagy (2000), *Ionospheres: Physics, Plasma Physics, and Chemistry*, Cambridge Univ. Press, Cambridge, U. K.

Sharp, R. D., W. Lennartsson, and R. J. Strangeway (1985), The ionospheric contribution to the plasma environment in near-earth space, *Radio Sci.*, *20*, 456–462.

Shay, M. A., and M. Swisdak (2004), Three-species collisionless reconnection: Effect of $O^+$ on magnetotail reconnection, *Phys. Rev. Lett.*, *93*(17), 175001−+, doi:10.1103/PhysRevLett.93.175,001.

Shelley, E. G., R. G. Johnson, and R. D. Sharp (1972), Satellite observations of energetic heavy ions during a geomagnetic storm, *J. Geophys. Res.*, *77*, 6104–6110.

Strangeway, R. J., C. T. Russell, C. W. Carlson, J. P. McFadden, R. E. Ergun, M. Temerin, D. M. Klumpar, W. K. Peterson, and T. E. Moore (2000), Cusp field-aligned currents and ion outflows, *J. Geophys. Res.*, *105*, 21129, doi:10.1029/2000JA900032.

Tóth, G., et al. (2005), Space weather modeling framework: A new tool for the space science community, *J. Geophys. Res.*, *110*, A12226, doi:10.1029/2005JA011126.

Wang, H., A. J. Ridley, and H. Luhr (2008), Validation of the space weather modeling framework using observations from champ and dmsp, *Space Weather*, *6*, S03001, doi:10.1029/2007SW000355.

Wiltberger, M., W. Wang, A. Burns, S. Solomon, J. Lyon, and C. Goodrich (2004), Initial results from the coupled magnetosphere ionosphere thermosphere model: Magnetospheric and ionospheric responses, *J. Atmos. Sol.-Terr. Phys.*, *66*, 1411–1423.

Winglee, R. M. (2000), Mapping of ionospheric outflows into the magnetosphere for varying IMF conditions, *J. Atmos. Terr. Phys.*, *62*, 527–540.

Winglee, R. M., D. Chua, M. Brittnacher, G. K. Parks, and G. Lu (2002), Global impact of ionospheric outflows on the dynamics of the magnetosphere and cross-polar cap potential, *J. Geophys. Res.*, *107*(A9), 1237, doi:10.1029/2001JA000214.

Zhang, J., et al. (2007), Understanding storm-time ring current development through data-model comparisons of a moderate storm, *J. Geophys. Res.*, *112*, A04208, doi:10.1029/2006JA011846.

A. Glocer, NASA/GSFC, Code 673, Greenbelt, MD 20771, USA. (alex.glocer-1@nasa.gov)

T. Gombosi, G. Tóth, and D. Welling, Department of Atmospheric Oceanic and Space Sciences, University of Michigan, Space Research Building, 2455 Hayward Street, Ann Arbor, MI 48109-2143, USA.